Journal of Alloys and Compounds 500 (2010) 145–148

Contents lists available at ScienceDirect

Journal of Alloys and Compounds

journal homepage: www.elsevier.com/locate/jallcom

Influence of quasicrystalline phase on transport processes in $Zr_{70}Pd_{30}$ amorphous alloy

Krystyna Pękała*, Jerzy Antonowicz, Piotr Jaśkiewicz, Tomasz Drobiazg, Jan Konupek

Faculty of Physics, Warsaw University of Technology, Koszykowa 75, 00-662 Warsaw, Poland

ARTICLE INFO

Article history:
Received 22 February 2010
Received in revised form 22 March 2010
Accepted 31 March 2010
Available online 7 April 2010

Keywords:
Amorphous materials
Quasicrystals
Electronic transport
X-ray diffraction
Calorimetry

ABSTRACT

Electron transport and structural properties of amorphous $Zr_{70}Pd_{30}$ alloy are investigated by electrical resistivity, thermoelectric power, differential scanning calorimetry and X-ray diffraction methods. It was found that appearance of the icosahedral quasicrystalline phase in the first crystallization stage contributes to an increase of the electrical resistivity and Seebeck coefficient. Temperature variation of transport properties in amorphous phase excludes a variable range hopping model, which supplies unreasonable values of hopping energy and hopping distance. A similar degree of agreement between experimental results and both the Ziman and weak localization models is found for the electrical resistivity. However, a relatively high content of early transition Zr atoms in the alloy points rather that the weak localization may play a role.

1. Introduction

Icosahedral quasicrystalline phase (QC) [1] as a primary devitrification product was observed in numerous multicomponent Zr-based metallic glasses [2–5]. However formation of quasicrystals in a case of binary Zr-bearing systems is limited to Zr–Pd and Zr–Pt systems [6,7]. Precipitation of quasicrystals was studied extensively for $Zr_{70}Pd_{30}$ and $Zr_{80}Pt_{20}$ glasses [6,8,9]. The tendency towards formation of the QC phase was explained by close correlation between atomic order in the glassy and quasicrystalline state [10–12]. A significant number of icosahedral-like clusters centered around Zr atoms present in the as-quenched state of amorphous $Zr_{70}Pd_{30}$ alloy were suggested to facilitate precipitation of the QC phase [11]. The icosahedral-like short range in Zr–Pd and Zr–Pt glasses was attributed to strong atomic bonding present in those systems [13]. The QC phase is a metastable product of devitrification of glassy $Zr_{70}Pd_{30}$ and transforms into tetragonal Zr_2Pd equilibrium phase on annealing [6].

Physical properties of QCs are remarkably different as compared to the constituent metallic elements. QCs exhibit high electrical resistivity sometimes comparable with that of insulators. The temperature coefficient of resistivity (TCR) is negative—in agreement with Mooij correlation [14]. The relatively large thermoelectric power and low thermal conductivity result in the high figure of merit ZT close to that of semiconductors [15] which enables to use QCs for thermoelectric devices for refrigeration and power generation. Moreover, the mechanical properties, corrosion resistance and thermal stability of QCs are superior than for semiconductors [16]. High electrical resistivity of QCs is caused by the gap at the Fermi level, which involves a low electron density in this energy range. The density of states shows very spiky structures and a width of peaks is of the order of 10–20 meV [17]. It was observed that thermoelectric power of QCs varies strongly and nonsystematically even at small changes of the Fermi energy occurring due to the composition variation [18]. Electrical resistivity and thermoelectric power (TEP) measurements are very sensitive experimental techniques which can be successfully applied to analysis of crystallization of metallic glasses [19–21]. In this study we apply those methods to investigate quasicrystal-forming $Zr_{70}Pd_{30}$ amorphous alloy.

Previous experimental studies of electron transport in $Zr_{70}Pd_{30}$ alloy were made only at low temperatures. Gruzalski et al. [22] interpreted the electrical resistivity with a modified Ziman model. Panova et al. [23] have studied electrical resistivity of amorphous, quasicrystalline and polycrystalline $Zr_{70}Pd_{30}$ alloy between 2 and 300 K. The temperature variation of TEP and Hall effect measurements were reported by Fritsch et al. [24]. The positive Hall constant was explained by a hybridization of the *s–d* states and the negative value of dE/dk at the Fermi level. Moreover the UPS spectra reveal a well separated 4*d* Pd and 4*d* Zr bands [25]. The 4*d* Zr band is located at the Fermi level and may strongly affect the electron transport processes in the $Zr_{70}Pd_{30}$ amorphous alloy. This paper is focused on a detailed investigation of the electron transport processes in a broad temperature range where formation of quasicrystalline and

* Corresponding author.
E-mail address: pekala@mech.pw.edu.pl (K. Pękała).

0925-8388/$ – see front matter © 2010 Elsevier B.V. All rights reserved.
doi:10.1016/j.jallcom.2010.03.243

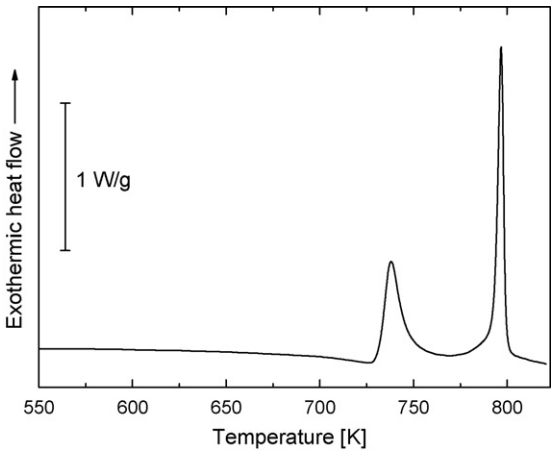

Fig. 1. DSC scan of as-quenched $Zr_{70}Pd_{30}$ taken at 20 K/min.

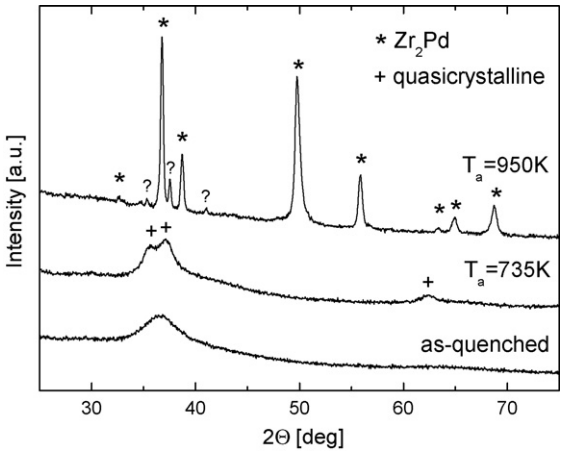

Fig. 2. XRD spectra of $Zr_{70}Pd_{30}$ alloy in as-quenched state, after isochronal annealing up to 735 and 950 K. Bragg peaks of icosahedral quasicrystalline and tetragonal Zr_2Pd phases are indicated.

crystalline phases occurs. According to our knowledge this paper is the first report on the electrical resistivity and thermoelectric power in $Zr_{70}Pd_{30}$ amorphous alloy at high temperatures.

2. Experimental

Ingots of $Zr_{70}Pd_{30}$ alloy were prepared from pure elements in arc-melting furnace applying multiple remelting to ensure homogeneity. The investigated samples were prepared using single roller melt spinning setup operating in argon atmosphere. The resulting ribbons were about 25 μm thick and 1.5 mm wide. The electrical resistivity measurements were carried out by means of DC four-probe method. The thermoelectric power (TEP) was measured by differential method. Both experiments were carried out in vacuum (10^{-6} mbar) under continuous heating conditions (20 K/min). The differential scanning calorimetry (DSC) measurements were performed using Q200 device (TA Instruments) operating under nitrogen flow. The X-ray diffraction (XRD) analysis of as-quenched and thermally treated samples was performed using Philips X'Pert Pro diffractometer (CuKα radiation).

3. Results

The evolution of a DSC signal of an as-quenched $Zr_{70}Pd_{30}$ taken at 20 K/min is shown in Fig. 1. A glass transition point can be observed in the DSC curve around 700 K. The presence of two distinct exothermic events attributed to two stages of crystallization are consistent with previously published data [6,9]. The crystallization onset point is located at 727 K. The two DSC maxima are located at 738 and 797 K, respectively. The heat release due to the first crystallization event was found to be equal to 23 J/g while the value of 29 J/g was obtained in case of the second peak. The results of the XRD analysis of as-quenched and annealed samples are demonstrated in Fig. 2. The "halo" spectrum for the as-quenched sample proves the fully amorphous character of the melt spun ribbons used in present study. The sample preheated up to 735 K exhibits presence of significantly broadened peaks corresponding to icosahedral nanoquasicrystalline phase with grain size less than 20 nm [26] resulting from the first transformation stage. At this stage the amorphous alloy transforms overwhelmingly to QC phase in agreement with results of Saida et al. [26]. For the sample annealed up to 950 K the XRD spectrum consists predominantly of Bragg reflexes attributed to Zr_2Pd phase which is consistent with data available in the literature [9,6]. A relatively high electrical resistivity of the amorphous $Zr_{70}Pd_{30}$ alloy equal to 228 μΩ cm at room temperature (Fig. 3) is in good agreement with data available in the literature [27]. The temperature coefficient of electrical resistivity (TCR) of the glassy phase equals to $-0.8 \times 10^{-4}\,K^{-1}$. Above room temperature the electrical resistivity is a weakly varying function of temperature (Fig. 3) and exhibits a minimum at 727 K coinciding with the first crystallization onset, as revealed by the DSC spectra. The subsequent resistivity increase is due to the transformation from the homogeneous amorphous structure to a composite consisting mainly of the quasicrystalline grains. The electrical resistivity of the composite becomes enhanced because of high resistivity of QC phase and due to additional grain boundary resistivity component. The resistivity increases up to 763 K when a sudden drop occurs indicating the beginning of the second crystallization stage. This is followed by a gradual resistivity decrease observed up to 930 K. The resistivity suppression above 763 K occurs during the polymorphic crystallization to the polycrystalline phase when the restored atomic long range ordering facilities electron propagation. Above 930 K the resistivity grows continuously with temperature as expected for crystalline metals and exhibits a positive TCR. Such a behavior proves that the crystallization processes are completed at 930 K. Thermoelectric power (Seebeck coefficient) was measured both for as-quenched sample as well as for a sample annealed up to 950 K (Fig. 4). TEP of the as-quenched alloy is positive and relatively low (below 2 μV/K) and increases slowly up to 620 K. Then one observes that TEP starts to drop at 700 K which corresponds to the glass transition as determined from DSC spectra, and finally TEP reaches a local minimum at crystallization threshold temperature of 727 K (see inset in Fig. 4). The region of growing TEP (727–763 K) matches well the DSC and electrical resistivity data for the first crystallization stage. The subsequent decrease of TEP is related to initiation and completion

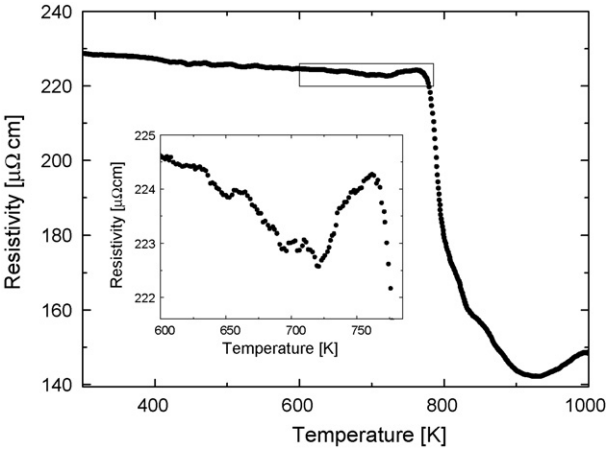

Fig. 3. Variation of electrical resistivity of as-quenched $Zr_{70}Pd_{30}$ during continuous heating at 20 K/min. The inset shows temperature interval around crystallization onset point.

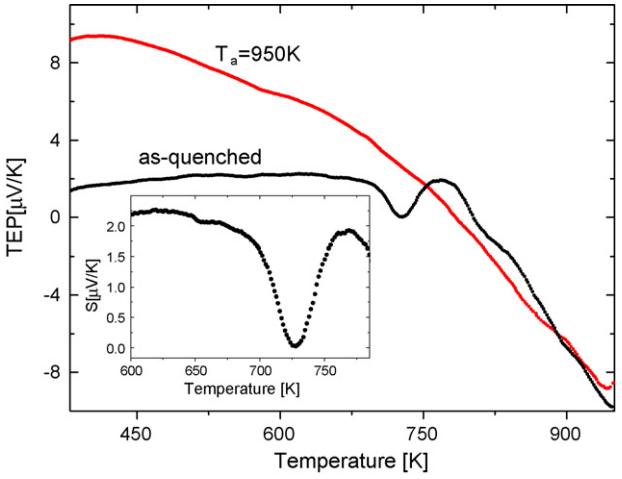

Fig. 4. Thermoelectric power of $Zr_{70}Pd_{30}$ alloy in as-quenched state (black curve) and after isochronal annealing (20 K/min) up to 950 K (red curve) measured during continuous heating at 20 K/min. The inset shows temperature interval around crystallization onset point. (For interpretation of the references to color in this figure legend, the reader is referred to the web version of the article.)

of the second stage of crystallization. At higher temperatures TEP changes a sign about 800 K and finally reaches −10 μV/K at 950 K. The thermoelectric power measurement of sample heated up to 950 K at 20 K/min and then cooled down to room temperature is represented by the red curve in Fig. 4. The value of TEP for the annealed sample starts to decrease from 9.3 μV/K at lower temperature range. Above 750 K TEP of the crystalline alloy obtained by annealing up to 950 K coincides with the TEP curve for the non-annealed one. This shows that the as-quenched alloy heated to 750 K at 20 K/min has the polycrystalline structure appearing during the second crystallization stage.

4. Analysis of electrical resistivity and thermoelectric power data

The electrical resistivity of the $Zr_{70}Pd_{30}$ alloy studied is relatively high and diminishes at elevated temperatures. Such a behavior is characteristic for metallic glasses with a high content of early transition metals. The electron transport processes are governed by the 4*d* electrons of Zr appearing at the Fermi level, whereas the *d* electrons of Pd are located below E_F [28]. In order to identify the conduction mechanism the experimental results of electrical resistivity ρ are fitted to three models commonly applicable for metallic glasses. The most often applied the generalized Ziman model [25] predicts the following relation in a temperature range above the Debye temperature T_D [29]:

$$\rho(T) = \rho_0 + AT \quad (1)$$

where ρ_0 and A are constant parameters. The sign and value of the A parameter is determined by the temperature variation of the structural factor. The A parameter becomes negative when $2k_F = k_P$, where k_F and k_P are Fermi vector and maximum of the structure factor, respectively. Gruzalski et al. [22] demonstrated that this condition is obeyed when about 2 and about 1 electrons are contributed to conduction band from Zr and Pd, respectively. Numerical fitting of resistivity to Eq. (1) supplies the parameters ρ_0 and A equal to 232.4 μΩ cm and −0.013 μΩ cm K^{-1}, respectively. The results are plotted in Fig. 5a.

On the other hand, the Mott coefficient $G = 200/\rho$ describing a degree of localization [29] estimated to be equal to 0.94 suggests that the weak localization processes may play a role. When a temperature is raising the weak localization effect is gradually

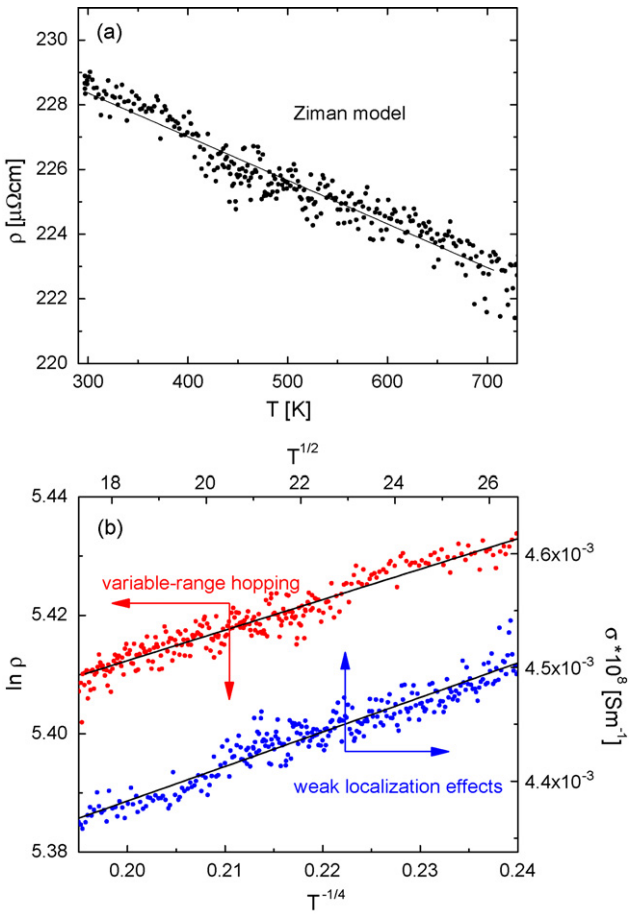

Fig. 5. Electrical resistivity data (points) fitted with different conduction models (solid lines). Top: Ziman model (Eq. (1)). Bottom: weak localization effects (blue curve, Eq. (2)), variable hopping range conductivity (red curve, Eq. (3)). For details see text. (For interpretation of the references to color in this figure legend, the reader is referred to the web version of the article.)

destroyed by the inelastic electron–phonon scattering. Then above $T_D/3$ the conductivity $\sigma = 1/\rho$ obeys a relation [30]:

$$\sigma(T) = \sigma_0 + BT^{1/2} \quad (2)$$

where B and σ_0 are constants. Values of σ_0 and B derived from a fitting to resistivity results (Fig. 5b) are equal to 417×10^{-3} S m^{-1} and 1.17×10^{-3} S m^{-1} $K^{-1/2}$, respectively. As the short range icosahedral ordering exists in the amorphous phase the variable range hopping conductivity may be accounted for by the formula [31]:

$$\rho(T) = \rho_0 \exp\left(\frac{T_0}{T}\right)^{1/4} \quad (3)$$

where ρ_0 and T_0 are constants. The ρ_0 and T_0 parameters derived from a fitting to Eq. (3) are equal to 202 μΩ cm and 0.070 K, respectively (Fig. 5b). Hence the average hopping distance may be estimated as:

$$r = a_B\left(\frac{T_0}{T}\right)^{1/4} \quad (4)$$

where a_B – Bohr radius, to be 0.0065 and 0.0053 nm at 300 and 700 K, respectively. These hopping distances are much smaller than interatomic spacing and show that the variable range hopping model is inappropriate for alloy studied. This conclusion is additionally supported by the relatively low hopping energies $\varepsilon = (T^3T_0)^{1/4}$ spread from 37 to 70 K between the room temperature and 700 K.

After disproving the hopping mechanism it is hard to select the better of the remaining models when applying only correlation coefficients, which are close being equal to 0.91 and 0.92 for the Ziman and weak localization approaches, respectively. For the more advanced comparison of the two models the temperature dependence of structural factor for the A parameter of Eq. (1) and the temperature variation of the electron mean free path for B parameter of Eq. (2) are required. Unfortunately such a data are not available. Thus, one may conclude that the Ziman model is relatively less satisfactory as it was also reported for similar alloys (Zr–Cu and Zr–Ni) with high content of early transition metals [29].

The electrical resistivity increase observed during the first crystallization stage between 727 and 763 K reveals an abrupt formation of the QC phase occurring in this relatively narrow temperature interval. The rising QC fraction enhances the measured resistivity due to two factors. First of all the electrical resistivity of QC phase is high due to the energy gap near the Fermi level [17] and nanometric grain size [20]. Moreover a large density of small quasicrystal grains (below 20 nm [6]) generates the additional resistivity component due to the electron scattering on the grain boundaries.

The approximately linear temperature variation of thermoelectric power up to 660 K agrees with the Mott relation [32]:

$$S = -\frac{\pi^2 k^2 T}{3\,|e|\,E_F}\left[\frac{\partial \log \sigma}{\partial E}\right]_{E=E_F} \quad (5)$$

The positive values of TEP suggest that the additional term related to localization effects should be taken into account [33]. The local TEP decrease at 700 K in vicinity of glass transition temperature has not been reported previously in metallic glasses. The following recovery of TEP at about 727 K is due to a formation of the QC phase with a positive TEP. Such TEP behavior coinciding with the resistivity enhancement above 727 K confirms the semiconductor-like properties of the QC phase [23].

5. Conclusions

The electrical resistivity and thermoelectric power of amorphous $Zr_{70}Pd_{30}$ alloy measured at elevated temperatures are correlated to the quasicrystalline and polycrystalline phases emerging in this range. The glass transition is well pronounced in the temperature variation of the thermoelectric power which is reported for the first time. It is found that a growth of the quasicrystalline phase starting at 727 K causes a discernible increase in the electrical resistivity and thermoelectric power. The second crystallization stage starting at 763 K leads to resistivity decrease when the long range ordering is restored. Analysis of transport properties in amorphous phase excludes a variable range hopping model, which supplies unreasonable values of hopping energy and hopping distance. A similar degree of agreement between experimental results and both the Ziman and weak localization models is found for the electrical resistivity. However, a relatively high content of early transition Zr atoms in the alloy points rather that the weak localization may play a role.

Acknowledgments

Professor A.R. Yavari of SIMAP (Grenoble) is kindly acknowledged for providing the samples used in this study. This work was supported by a grant of Faculty of Physics of Warsaw University of Technology.

References

[1] D. Shechtman, I. Blech, D. Gratias, J.W. Cahn, Phys. Rev. Lett. 53 (1984) 1951–1953.
[2] D.V. Louzguine-Luzgin, A. Inoue, Annu. Rev. Mater. Sci. 38 (2008) 403–423.
[3] U. Köster, J. Meinhardt, S. Roos, H. Liebertz, Appl. Phys. Lett. 69 (1996) 179–181.
[4] V. Dmitri, Appl. Phys. Lett. 78 (2001) 1841–1843.
[5] J. Saida, E. Matsubara, A. Inoue, Mater. Trans. JIM 44 (2003) 1971–1977.
[6] J. Saida, M. Matsushita, A. Inoue, J. Appl. Phys. 90 (2001) 4717–4724.
[7] J. Saida, T. Sanada, S. Sato, M. Imafuku, C. Li, A. Inoue, Z. Kristallogr. 223 (2008) 726–730.
[8] J. Saida, E. Matsubara, A. Inoue, Appl. Phys. Lett. 88 (2000) 6081–6083.
[9] B.S. Murty, D.H. Ping, K. Hono, Appl. Phys. Lett. 77 (2000) 1102–1104.
[10] J. Saida, M. Matsushita, A. Inoue, Appl. Phys. Lett. 79 (2001) 412–414.
[11] T. Takagi, T. Ohkubo, Y. Hirotsu, B.S. Murty, K. Hono, D. Shindo, Appl. Phys. Lett. 79 (2001) 485–487.
[12] K. Saksl, H. Franz, P. Jovari, K. Klementiev, E. Welter, A. Ehnes, J. Saida, A. Inoue, J.Z. Jiang, Appl. Phys. Lett. 83 (2003) 3924–3926.
[13] T. Nakamura, E. Matsubara, M. Sakurai, M. Kasai, A. Inoue, Y. Waseda, J. Non-Cryst. Solids 312–314 (2002) 517–521.
[14] J.H. Mooij, Phys. Stat. Sol. (a) 17 (1973) 521–530.
[15] F. Cyrot-Lackmann, Mat. Sci. Eng. A 294–296 (2000) 611–612.
[16] H.-R. Trebin, Quasicrystals: Structure and Physical Properties, Wiley–VCH, Weinheim, 2003.
[17] E. Maciá, Phys. Rev. B 61 (2000) 8771–8777.
[18] T. Fujiwara, S. Yamamoto, G. Trambly de Laissardière, Phys. Rev. Lett. 71 (1993) 4166–4169.
[19] K. Pękała, J. Latuch, P. Jaśkiewicz, L. Nowiński, J. Antonowicz, J. Metastable Nanocryst. Mater. 20–21 (2004) 494–498.
[20] K. Pękała, J. Non-Cryst. Solids 353 (2007) 888–892.
[21] K. Pękała, J. Non-Cryst. Solids 354 (2008) 5304–5307.
[22] G.R. Gruzalski, J.A. Gerber, D.J. Sellmyer, Phys. Rev. B 19 (1979) 3469–3475.
[23] G.Kh. Panova, N.A. Chernoplekov, A.A. Shilpov, Phys. Solid State 47 (2005) 1205–1210.
[24] G. Fritsch, E. Luescher, A. Schulte, A. Eckert, J. Willer, W. Dyckhoff, J. Non-Cryst. Solids 61/62 (1984) 1225–1230.
[25] J.M. Ziman, Philos. Mag. 6 (1961) 1013.
[26] J. Saida, M. Matsushita, A. Inoue, J. Alloys Compd. 342 (2002) 18–23.
[27] M. Kullik, G. von Minnigerode, K. Samwer, Z. Phys. B 60 (1985) 357–362.
[28] J. Kübler, K.H. Bennemann, R. Lapka, F. Rösel, P. Oelhafen, H.-J. Güntherodt, Phys. Rev. B 23 (1981) 5176–5184.
[29] U. Mizutani, Introduction to the Electron Theory of Metals, Cambridge University Press, 2001.
[30] M.A. Howson, J. Phys. F 14 (1984) L25–L31.
[31] V.F. Gantmakher, Electron and Disorder in Solids, Clarendon Press, Oxford, 2005.
[32] D.K.C. MacDonald, Thermoelectricity, Dover, New York, 2006.
[33] A.B. Kaiser, Phys. Rev. B 35 (1987) 2480–2483.